Supporting information file for "Rate constants for the N(^{4}S) + CH($X^2\Pi_r$) reaction. Implications for N_2 formation cycles in dense interstellar clouds."

S-I. POTENTIAL ENERGY SURFACES

To study the title reaction, global potential energy surfaces (PESs) of the lowest two triplet ($1^3A'$ and $1^3A''$) states of HCN have been determined. The electronic structure calculations were performed at the internally contracted multi-reference configuration interaction level with the Davidson correction (MRCI + Q),[1,2,3] based on（$1^3A'$, $2^3A'$ and $1^3A''$) state-averaged completed active space self-consistent field (CASSCF) wavefunctions. The full-valence active space with 10 electrons distributed in 9 orbitals was used, with the 1s orbitals of the carbon and nitrogen kept doubly occupied but fully optimized. All *ab initio* calculations were carried out with the MOLPRO 2010 package.[4]

The HCN molecule was treated in C_s symmetry and the PESs are described in an internal coordinate (r_{CH}, r_{CN}, $\theta_{H\text{-}C\text{-}N}$) grid. To reduce computational costs, we adopted the hierarchical construction scheme suggested by Fu *et al.*[5] to construct the PESs. Low-accuracy PESs were first constructed using the aug-cc-pVTZ (AVTZ) basis set and then improved to the high-accuracy ones using the aug-cc-pV5Z (AV5Z) basis set. For the low-accuracy PESs, we used 35 points for r_{CH} from 1.3 to 13.0 a_0 and 49 points for r_{CN} varied in the interval [1.3, 15.0 a_0]. For the $\theta_{H\text{-}C\text{-}N}$ angle, 22 points were used from 0 to 180°. This set of grids gives a total of about 37000 symmetry-unique points. With the larger AV5Z basis set, the grid in each coordinate was reduced by about a factor of 2, resulting in 4240 grid points. The differences between the

corresponding low and high-accuracy PESs, $\Delta V_{\text{high-low}}$, which are smoother functions of the nuclear coordinates, were fit with the cubic spline method. By adding the difference potential $\Delta V_{\text{high-low}}$ to the low-accuracy PESs, the high-accuracy PESs were obtained:

$$V_{\text{high}} = V_{\text{low}} + \Delta V_{\text{high-low}} \quad (1)$$

Compared to the direct calculation of 37000 points of MRCI + Q/AV5Z energies, this method reduced the total computational time required by about a factor of 8.

Table S-I summarizes the *ab initio* energies and geometries of stationary points on each PES together with the previous theoretical results. It is shown that only slight differences exist in molecular structures between the AV5Z and AVTZ PESs. However, the AV5Z PESs have larger exothermal energies (4.11 and 2.99 eV for $1^3A'$ and $1^3A''$ respectively) than the AVTZ PESs (3.92 and 2.82 eV), representing a better agreement with the experimental values (4.26 and 3.11 eV as cited in Ref. 6). Below, only the high-accuracy PESs are discussed.

The stationary point geometries obtained in this work are in qualitative agreement with several previous theoretical studies, but quantitative differences do exist. Comparing with the HCN equilibrium geometries on the $1^3A'$ state reported by Rayez *et al.*,[6] for example, our structure is 0.028 a_0 shorter for the C-H bond, 0.038 a_0 shorter for the C-N bond and 0.8° smaller for the bond angle, but in a better agreement with the more reliable CCSD(T)/AV5Z results (2.081, 2.433, 120.6°).[7] Our HCN structure is also in good agreement with the recent CASPT2/ANO-L results of Li *et al.*[8] for both electronic states.

The PESs for both electronic states have two deep wells corresponding to the HCN and HNC isomers separated by an isomerization barrier as shown in Fig. 1 of the main article. Fig. S1 shows contour plots of the $1^3A'$ and $1^3A''$ PESs with two fixed bond angles corresponding to the HCN and HNC minima on the two PESs.

S-2. QUANTUM DYNAMICS

In this work, the Chebyshev real wave packet method[9] was employed to study reaction dynamics. Since the details can be found from our previous publications,[9,10,11] only a brief description is given here. The Hamiltonian in the reactant Jacobi coordinates (R, r, γ) is given by ($\hbar = 1$):

$$\hat{H} = -\frac{1}{2\mu_R}\frac{\partial^2}{\partial R^2} - \frac{1}{2\mu_r}\frac{\partial^2}{\partial r^2} + \frac{(\hat{J}-\hat{j})^2}{2\mu_R R^2} + \frac{\hat{j}^2}{2\mu_r r^2} + V(R,r,\gamma), \quad (2)$$

where $\boldsymbol{r}$ is the vector from the C atom to the H atom, $\boldsymbol{R}$ is the vector pointing to the N atom from the center of the mass of the diatom CH and γ is the enclosed angle between the two vectors. μ_r and μ_R are the diatomic CH and overall reduced masses, respectively. Here, $\hat{J}$ and $\hat{j}$ represent the total and diatomic CH rotational angular momentum operators, respectively. Since the spin and electronic angular momenta were ignored, j corresponds to the rotational quantum number of CH($X\,^2\Pi$), which is more commonly denoted by N-1.

For each given total angular momentum J and parity p, the wave function in the BF frame can be written as:

$$\left|\Psi^{Jp}\right\rangle = \sum_{\alpha_r \alpha_R jK} C^{Jp}_{\alpha_r \alpha_R jK} \left|\alpha_r\right\rangle \left|\alpha_R\right\rangle \left| jK, Jp\right\rangle, \quad (3)$$

where K is the projection of J onto the BF z axis. The Hamiltonian and wave function were discretized in a mixed grid/basis representation[10] including a discrete variable

representation (DVR)[12] for the two radial degrees of freedom and a finite basis representation (FBR) for the angular degrees of freedom. For the radial degrees of freedom, we used a *L*-shaped grid method,[13,11] which saved a large number of grid points. The grids of two radial Jacobi coordinates are indexed respectively by α_r and α_R. The parity-adapted angular basis can be expanded as

$$\left| jK; Jp \right\rangle = (2 + 2\delta_{K,0})^{-1/2} (\left| JK \right\rangle \left| jK \right\rangle + p(-1)^J \left| J - K \right\rangle \left| j - K \right\rangle), \quad (4)$$

where $\left| jK \right\rangle \equiv Y_j^K(\gamma, 0)$ are normalized associated Legendre polynomials and $\left| JK \right\rangle \equiv \sqrt{(2J+1)/8\pi^2} D_{KM}^J$ are normalized Wigner (D_{KM}^J) rotation matrices.[14]

In the space-fixed (SF) frame, The initial wave packet $\left| \Psi_i \right\rangle$ was defined below:[10]

$$\left| \Psi_i \right\rangle = N e^{-(R-R_0)^2/2\delta^2} \cos k_0 R \left| \varphi_{v_i j_i} \right\rangle \left| j_i l_i, Jp \right\rangle, \quad (5)$$

where *N* is the normalization factor, R_0 and δ represent respectively the initial position and width of the Gaussian function, $k_0 = \sqrt{2\mu_R E_0}$ is the mean momentum and $\left| \varphi_{v_i j_i} \right\rangle$ (v_i=0, j_i=0) is the eigenfunction of the initial rovibrational state of CH. The initial wave function was transformed into the BF frame before propagation.

The wave packet $\left| \Psi_k \right\rangle$ was propagated using the modified Chebyshev recursion relation:[15]

$$\left| \Psi_k \right\rangle = 2D\hat{H}_s \left| \Psi_{k-1} \right\rangle - D^2 \left| \Psi_{k-2} \right\rangle, \qquad k \geq 2, \quad (6)$$

where *D* is a boundary damping function. The iteration begins with $\left| \Psi_0 \right\rangle = \left| \Psi_i \right\rangle$ and $\left| \Psi_1 \right\rangle = D\hat{H}_s \left| \Psi_0 \right\rangle$. $\hat{H}_s$ is defined as

$$\hat{H}_s = (\hat{H} - H^+)/H^- \quad (7)$$

to scale the Hamiltonian to (-1,1). H^+ and H^- are respectively the spectral

medium and half width of the Hamiltonian, which can be calculated from the upper and lower spectral limits of the Hamiltonian ($H_{\max}$ and $H_{\min}$) with the relation $H^{\pm} = (H_{\max} \pm H_{\min})/2$.

To carry out final state projection in the product channel, we used a reactant coordinate based method,[11, 16] which can extract state-to-state *S*-matrix elements ($S^{J}_{v_f j_f K_f \leftarrow v_i j_i K_i}(E)$) of product channels. Then the state-to-state integral cross sections (ICSs) can be computed as

$$\sigma_{v_f j_f \leftarrow v_i j_i}(E) = \frac{\pi}{(2j_i+1)k^2_{v_i j_i}} \sum_{K_i} \sum_{K_f} \sum_{J} (2J+1) \left| S^{J}_{v_f j_f K_f \leftarrow v_i j_i K_i}(E) \right|^2 , \quad (8)$$

in which $k_{v_i j_i}$ is the initial translational wave vector. The calculated ICSs are plotted as a function of collision energy in Fig. 2 of the main article.

Finally, the reaction rate constant of the specified initial reactants is a Boltzmann weighted average of ICSs over the collision energy:[10]

$$k_{v_i j_i}(T) = \frac{f_e(T)}{k_B T} \left(\frac{8}{\pi \mu_R k_B T}\right)^{1/2} \sum_{v_f j_f} \int_0^{\infty} \sigma_{v_f j_f \leftarrow v_i j_i}(E_c) e^{-E_c/k_B T} E_c dE_c , \quad (9)$$

where k_B is the Boltzmann constant, T is the temperature and the electronic statistical weighting factor $f_e(T)$ is written as

$$f_e(T) = \frac{gw(T)}{Q_{el}} = \frac{gw(T)}{4 \times [2 + 2\exp(-40.2/T)]} . \quad (10)$$

Here, g =3 is the degeneracy of the triplet states. For the ground and excited spin-orbit states of CH($X^2\Pi$) separated by 27.95 cm^{-1},[17] we have $w(T)$ = 1 and $w(T)$ = exp(-40.2/T), respectively.

The optimal numerical parameters listed in Table S-II were chosen by extensive convergence tests. For $J \leq 70$, a maximal K value of 20 converged the probabilities

well for each electronic state, and K_{max}=36 was sufficient for $70 \leq J \leq 95$. The Chebyshev propagation steps of 40000 and 28000 were needed for the $1^3A'$ and $1^3A''$ states to converge the total probabilities. Due to difficulties in damping the wave packet with long de Broglie wavelengths, reaction probabilities at very low collision energies (E_c< 0.02eV) may not converge completely. To converge cross sections up to 0.20 eV and rate constants up to 600 K, the maximum of J values of 80 and 95 were used for the $1^3A'$ and $1^3A''$ states, respectively. The reaction probabilities on the two electronic states are displayed in Fig. S2 as a function of the collision energy.

TABLE. S-I. Comparison of geometries (in bohr and degree) and energies (in eV) of the stationary points between our results and previous ones.

Stationary points	Property	$1^3A'$						
		This work AVTZ	This work AV5Z	Rayez *et al.*[6]	Nayak *et al.*[18]	Li *et al.*[8]	Fortenberry *et al.*[7]	Expt.[6]
N + CH	r_{CH}	2.10	2.10					
	ΔE	0	0					
H + CN	r_{CN}	2.231	2.221					
	ΔE	-3.92	-4.11	-4.13				-4.26
HCN minimum	r_{CH}	2.082	2.081	2.109	2.126	2.079	2.081	
	r_{CN}	2.458	2.447	2.485	2.481	2.453	2.433	
	$\theta_{H\text{-}C\text{-}N}$	121.9	121.5	122.3	121.9	121.7	120.6	
	ΔE	-4.85	-5.02	-4.40				
HNC minimum	r_{CN}	2.407	2.400	2.426				
	r_{NH}	1.964	1.959	1.986				
	$\theta_{H\text{-}N\text{-}C}$	111.3	111.5	110.2				
	ΔE	-4.32	-4.52	-3.84				
Isomerization saddle point	r_{CH}	2.391	2.429	2.415				
	r_{CN}	2.484	2.461	2.506				
	$\theta_{H\text{-}C\text{-}N}$	57.5	56.5	58.0				
	ΔE	-2.68	-2.83	-1.99				
H + NC saddle point	r_{CN}	2.271	2.259	2.305				
	r_{NH}	2.891	2.895	2.712				
	$\theta_{H\text{-}N\text{-}C}$	113.1	115.0	113.0				
	ΔE	-3.43	-3.63	-3.27				
H + CN saddle point	r_{CH}	3.33	3.31	3.143				
	r_{CN}	2.277	2.268	2.315				
	$\theta_{H\text{-}C\text{-}N}$	105.0	105.0	108.1				
	ΔE	-3.54	-3.73	-3.39				
Feature	Property	$1^3A''$						
		This work AVTZ	This work AV5Z	Rayez *et al.*[6]	Nayak *et al.*[18]	Li *et al.*[8]	Expt.[6]	
N + CH	r_{CH}	2.10	2.10					
	ΔE	0	0					

H + CN	r_{CN}	2.347	2.337				
	ΔE	-2.82	-2.99	-2.79			-3.11
HCN minimum	r_{CH}	2.101	2.098	2.143	2.099	2.103	
	r_{CN}	2.497	2.486	2.517	2.511	2.489	
	$\theta_{H\text{-}C\text{-}N}$	120.2	120.3	118.9	120.7	119.0	
	ΔE	-3.92	-4.09	-3.15			
HNC minimum	r_{CN}	2.653	2.652	2.676			
	r_{NH}	1.965	1.962	1.984			
	$\theta_{H\text{-}N\text{-}C}$	113.9	113.4	110.4			
	ΔE	-3.15	-3.31	-2.37			
Isomerization saddle point	r_{CH}	2.502	2.491	2.398			
	r_{CN}	2.669	2.661	2.770			
	$\theta_{H\text{-}C\text{-}N}$	53.0	53.0	55.0			
	ΔE	-1.78	-1.89	-0.95			
H + NC saddle point	r_{CN}	2.406	2.397	2.466			
	r_{NH}	2.841	2.832	2.640			
	$\theta_{H\text{-}N\text{-}C}$	117.7	117.8	118.0			
	ΔE	-2.25	-2.41	-1.75			
H + CN saddle point	r_{CH}	3.638	3.637	3.258			
	r_{CN}	2.360	2.350	2.392			
	$\theta_{H\text{-}C\text{-}N}$	116.8	116.6	117.2			
	ΔE	-2.70	-2.87	-2.42			

TABLE. S-II. Numerical parameters (in a.u.) used in the quantum mechanical wave packet calculations.

	$1^3A'$ state	$1^3A''$ state
Grid / basis ranges and sizes*	$R \in [0.5,\ 19.0],\ N_R^1 = 479,\ N_R^2 = 191$ $r \in [1.0,\ 13.5],\ N_r^1 = 99,\ N_r^2 = 29$ $\gamma \in [0,180°],\ j = 0 \sim j_{\max} = 90,\ N_j = 91$	$R \in [0.5,\ 15.0],\ N_R^1 = 374,\ N_R^2 = 149$ $r \in [1.0,\ 13.5],\ N_r^1 = 99,\ N_r^2 = 29$ $\gamma \in [0,\ 180°],\ j = 0 \sim j_{\max} = 74,\ N_j = 75$
Projection**	$R'_\infty = 8$	$R'_\infty = 8$
Initial wave packet	$R_0 = 15.0,\ \delta = 0.1,\ E_0 = 0.\ 05$ eV	$R_0 = 11.0,\ \delta = 0.15,\ E_0 = 0.1$ eV
Damping function	$D = \begin{cases} \exp[-0.012(\frac{R-15.3}{19.0-15.3})^2], & 15.3 \le R \le 19.0 \\ \exp[-0.2(\frac{r-12.5}{13.5-12.5})^2 - 0.028], & 12.5 < r \le 13.5 \\ \exp[-0.028(\frac{r-11.5}{12.5-11.5})^2], & 11.5 \le r \le 12.5 \\ 1, \text{ otherwise} \end{cases}$	$D = \begin{cases} \exp[-0.015(\frac{R-11.3}{15.0-11.3})^2], & 11.3 \le R \le 15.0 \\ \exp[-0.2(\frac{r-12.5}{13.5-12.5})^2 - 0.028], & 12.5 < r \le 13.5 \\ \exp[-0.028(\frac{r-11.5}{12.5-11.5})^2], & 11.5 \le r \le 12.5 \\ 1, \text{ otherwise} \end{cases}$
Spectral range	Potential energy cutoff: 8.0 eV Rotational kinetic energy cutoff: 6.0 eV	Potential energy cutoff: 8.0 eV Rotational kinetic energy cutoff: 6.0 eV
Propagation steps	40000	28000

* $N_{R/r}^1$ is the number of grid points in R/r, and $N_{R/r}^2$ is the number of R/r grid points in products/reactants region.

** R'_∞ is the H + CN product Jacobi coordinates.

FIG. S1. Contour plots of the HCN PESs in internal coordinates with the bond angle fixed. The $1^3A'$ and $1^3A''$ states are shown in the left and right panels, respectively. Upper panel: contour plots for the HCN minimum region; lower panel: contour plots for the HNC minimum region. The energy zero is defined at the N + CH asymptote and the contour intervals are 0.4 eV.

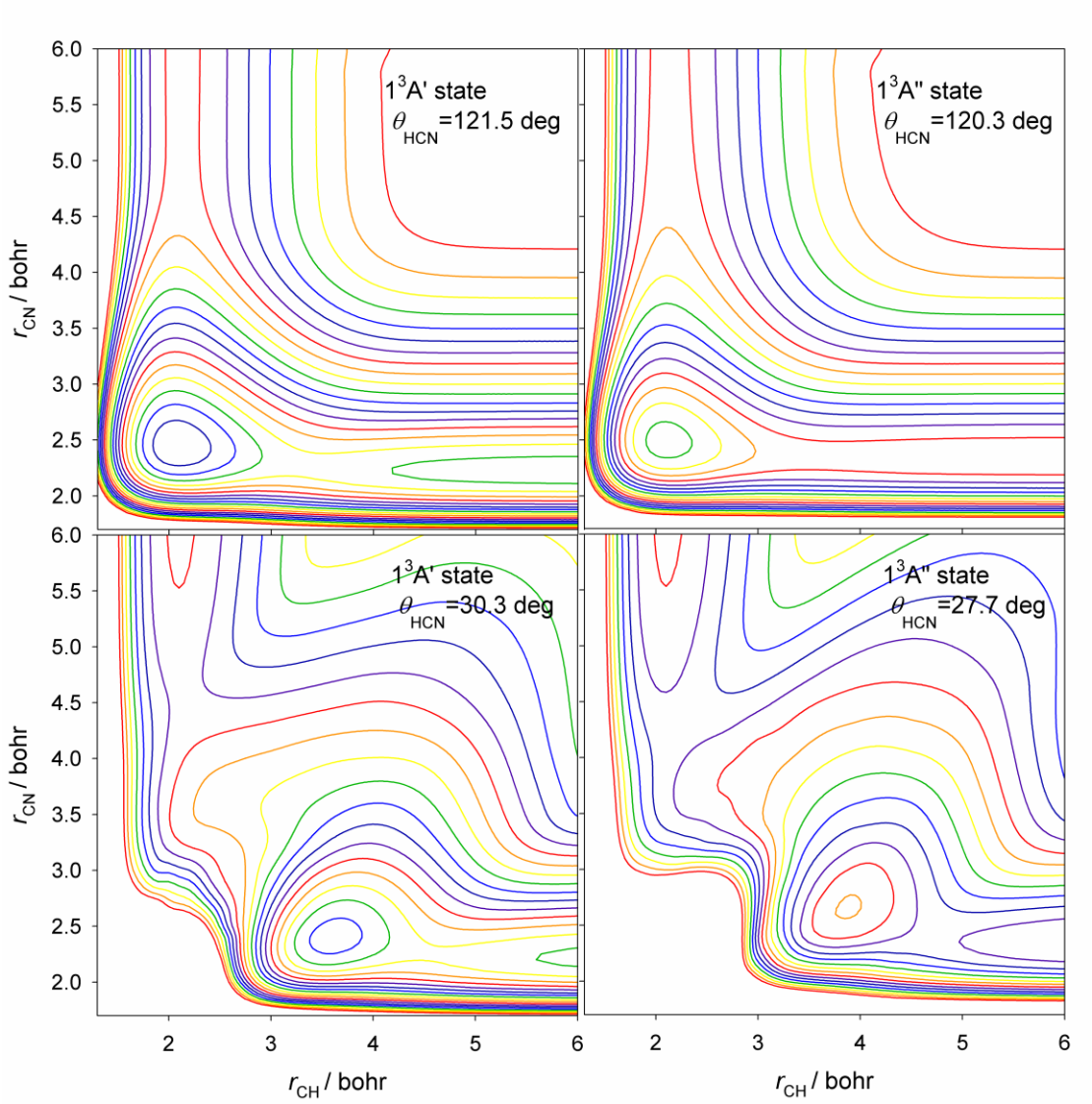

FIG. S2. Reaction probabilities (J=0, 20, 40, 60 and 80) for the $1^3A'$ and $1^3A''$ states as a function of collision energy (E_c).

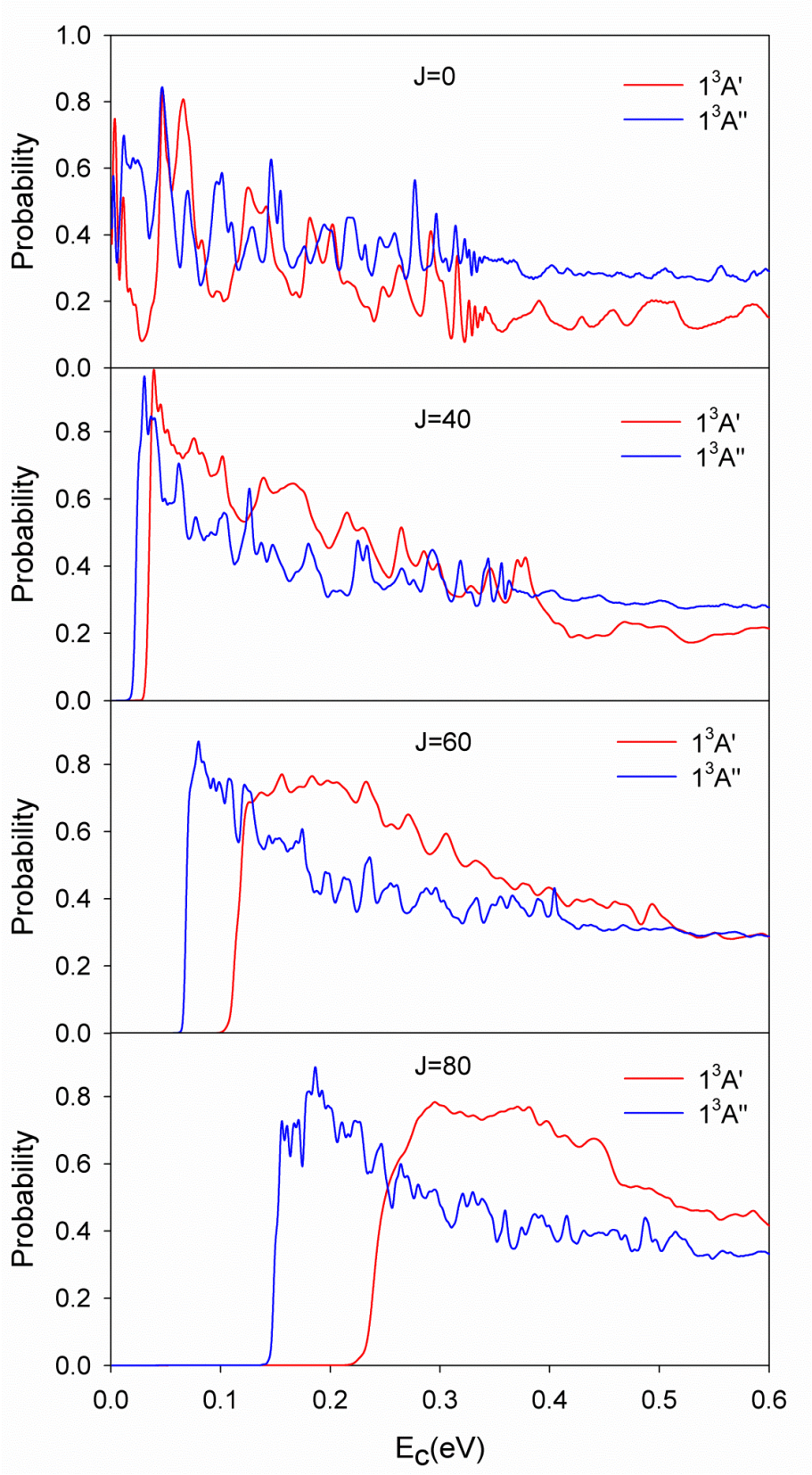

References:

1 S. R. Langhoff and E. R. Davidson, Int. J. Quantum. Chem. **8**, 61 (1974).

2 P. J. Knowles and H. J. Werner, Chem. Phys. Lett. **145**, 514 (1988).

3 H. J. Werner and P. J. Knowles, J. Chem. Phys. **89**, 5803 (1988).

4 H.-J. Werner, P. J. Knowles, G. Knizia, F. R. Manby, and M.schutz, MOLPRO,a package of *ab initio* programs (2010).

5 B. Fu, X. Xu, and D. H. Zhang, J. Chem. Phys. **129**, 011103 (2008).

6 M. T. Rayez, P. Halvick, J. C. Rayez, P. Millie, and B. Levy, Chem. Phys. **188**, 161 (1994).

7 R. C. Fortenberry, X. Huang, T. D. Crawford, and T. J. Lee, J. Phys. Chem. A **in press, DOI: 10.1021/jp309243s** (2012).

8 B.-T. Li, L.-L. Li, and H.-S. Wu, J. Comput. Chem. **33**, 484 (2012).

9 H. Guo, Int. Rev. Phys. Chem. **31**, 1 (2012).

10 S. Lin and H. Guo, Phys. Rev. A **74**, 022703 (2006).

11 Z. Sun, H. Guo, and D. H. Zhang, J. Chem. Phys. **132**, 084112 (2010).

12 J. C. Light and T. Carrington, Adv. Chem. Phys. **114**, 263 (2000).

13 R. C. Mowrey, J. Chem. Phys. **94**, 7098 (1991).

14 R. N. Zare, *Angular Momentum*. (Wiley, New York, 1988).

15 Z. Sun, S.-Y. Lee, H. Guo, and D. H. Zhang, J. Chem. Phys. **130**, 174102 (2009).

16 S. Gómez-Carrasco and O. Roncero, J. Chem. Phys. **125**, 054102 (2006).

17 K. P. Huber and G. Herzberg, *Molecular spectra and molecular structure*. (Van Nostrand Reinhold, New York, 1979).

18 M. K. Nayak, R. K. Chaudhuri, and S. N. L. G. Krishnamachari, J. Chem. Phys. **122**, 184323 (2005).